Cellular/Molecular

Alternative Splicing of the Flip/Flop Cassette and TARP Auxiliary Subunits Engage in a Privileged Relationship That Fine-Tunes AMPA Receptor Gating

Amanda M. Perozzo,[1,2] **Patricia M.G.E. Brown,**[1,2] **and Derek Bowie**[2]

[1]Integrated Program in Neuroscience, McGill University, Montréal, Quebec H3A 2B4, Canada and [2]Department of Pharmacology and Therapeutics, McGill University, Montréal, Quebec H3G 1Y6, Canada

Alternative splicing of AMPA-type glutamate receptors (AMPARs) and allosteric modulation by auxiliary subunits, such as transmembrane AMPAR regulatory proteins (TARPs), are two important mechanisms that regulate the time course of glutamatergic neurotransmission. Prior work has shown that alternative splicing of the flip/flop cassette profoundly regulates TARP γ2 modulation, where flip receptor gating exhibits robust sensitivity to TARPs while flop isoforms are relatively insensitive to TARP modulation. Whether this splice variant-specific regulation extends to other auxiliary subunit families, such as cornichons (CNIHs), GSG1L, or CKAMPs, remains unknown. Here, we demonstrate that CNIH-3 modulation is unaffected by AMPAR alternative splicing due to inherent differences in how CNIH-3 and TARP γ2 modify channel gating. CNIH-3 slows receptor deactivation from the outset of current decay, consistent with structural evidence showing its point of contact at the level of the pore. In contrast, TARP γ2 acts via the KGK site of the ligand-binding domain (LBD) to slow the onset of desensitization. Although GSG1L and CKAMP44 primarily slow recovery from desensitization, their effects on channel gating are unaffected by alternative splicing, further underlining that structural events leading to the onset and recovery from desensitization are separable. Together, this work establishes that alternative splicing and TARP auxiliary subunits form a unique partnership that governs fast glutamatergic signaling at central synapses. Since proteomic studies suggest that all native AMPARs co-assemble with at least two TARPs, allosteric coupling between the flip/flop cassette and TARPs may represent a common design element in all AMPAR complexes of the mammalian brain.

Key words: **alternative splicing; AMPA receptor; CKAMP44; cornichon; flip/flop cassette; GSG1L**

Significance Statement

All fast excitatory neurotransmission in the mammalian brain is mediated by AMPA-type glutamate receptors (AMPARs). The time course of AMPAR gating can be regulated by two distinct mechanisms: alternative splicing of the flip/flop cassette and association with auxiliary subunits. Although these regulatory mechanisms have been well studied individually, it is not clear whether alternative splicing impacts auxiliary protein modulation of AMPARs. Here, we compare the four main families of AMPAR auxiliary subunits, transmembrane AMPAR regulatory proteins (TARPs; γ2), cornichons (CNIH-3), GSG1L and CKAMPs (CKAMP44), and find a privileged relationship between TARPs and the flip/flop cassette that is not shared by others. The flop cassette acts as a master switch to override TARP action, and this coupling represents a way to fine-tune AMPAR signaling.

Received Dec. 14, 2022; revised Feb. 10, 2023; accepted Mar. 13, 2023.

Author contributions: A.M.P. and D.B. designed research; A.M.P. and P.M.G.E.B. performed research; A.M.P. and P.M.G.E.B. analyzed data; A.M.P. wrote the first draft of the paper; A.M.P., P.M.G.E.B., and D.B. edited the paper; A.M.P. and D.B. wrote the paper.

This work was supported by an operating grant from the Canadian Institutes of Health Research (CIHR). A.M.P. was supported by Natural Sciences and Engineering Research Council of Canada (NSERC) CGS-M and PGS-D fellowships. We thank all Bowie lab members, past and present, for critical discussion. We also thank Jakob von Engelhardt for kindly providing the CKAMP44 cDNA.

The authors declare no competing financial interests.

Correspondence should be addressed to Derek Bowie at derek.bowie@mcgill.ca.

https://doi.org/10.1523/JNEUROSCI.2293-22.2023

Introduction

Alternative splicing of precursor mRNA is a critical post-transcriptional modification that serves to diversify the proteome (Black, 2000) and is especially important in the nervous system across development and in the mature brain (Vuong et al., 2016). Alternative splicing regulates neuronal differentiation, axon guidance and synaptogenesis, as well as dictates the electrophysiological properties of individual neurons to fine-tune synaptic transmission (Lipscombe, 2005; Li et al., 2007). Both voltage-gated and ligand-gated ion channels are subject to alternative splicing in the nervous system (Hood and

Emeson, 2012; Herbrechter et al., 2021). This process impacts many facets of channel behavior, from ion conductance and activation/inactivation kinetics, to interactions with other proteins and downstream intracellular signaling (Grabowski and Black, 2001). For example, alternative splicing in neuronal voltage-gated calcium channels modifies the voltage-dependence of activation, which can profoundly influence calcium entry and thus gene expression, transmitter release, and synaptic plasticity (Lipscombe et al., 2013). This fundamental process of gene regulation is highly controlled both spatially and temporally; as such, dysfunction often leads to neurological disease (Dredge et al., 2001).

Alternative splicing in AMPA-type glutamate receptors (AMPARs) was first identified by the group of Peter Seeburg (Sommer et al., 1990; Seeburg, 1996). Splicing occurs in the four genes that encode the AMPAR pore-forming subunits at a site termed the "flip/flop cassette," which is within the ligand-binding domain (LBD; Fig. 1*A*,*B*). Alternative splicing yields two splice variants termed flip and flop (Sommer et al., 1990). The expression of GluA1–GluA4 flip and flop variants is cell-type specific and developmentally-regulated (Monyer et al., 1991). These subunit isoforms exhibit distinct pharmacological and biophysical properties, and also differ in their responsiveness to allosteric modulators such as cyclothiazide and external anions (Mosbacher et al., 1994; Partin et al., 1994, 1996; Swanson et al., 1997; Dawe et al., 2019). Moreover, splicing impacts AMPAR assembly and trafficking through the endoplasmic reticulum (ER; Coleman et al., 2006; Penn et al., 2008; Sukumaran et al., 2012). Since AMPARs mediate the majority of fast excitatory neurotransmission in the mammalian brain, AMPAR alternative splicing is likely to have significant consequences on homeostatic adaptation and the shaping of neuronal circuits (Trussell, 1997; Schmid et al., 2001; Orlandi et al., 2011; Penn et al., 2012).

AMPARs are subject to yet another level of complex regulation through their association with auxiliary subunits that directly impact their trafficking and functional properties (Jackson and Nicoll, 2011). Recent work from our lab has shown that alternative splicing affects AMPAR modulation by transmembrane AMPAR regulatory proteins (TARPs), which are thought to be bound to all native AMPARs (Schwenk and Fakler, 2021), by controlling the resting mobility of the AMPAR (Dawe et al., 2019). Resting mobility is determined by a single amino acid residue within the flip/flop cassette, Ser/Asn775, which controls motions in the distant N-terminal domain (NTD). Flip variants promote moderate NTD movement, which establishes slower channel desensitization and robust regulation by anions and TARP γ2 whereas greater NTD mobility imparted by the flop cassette precludes allosteric regulation. Whether alternative splicing similarly affects regulation by CNIHs, GSG1L, and CKAMPs has yet to be investigated.

Here, we show that alternative splicing of the flip/flop cassette distinguishes TARP γ2 from CNIH-3 modulation of AMPAR gating kinetics. We find that TARP γ2 primarily regulates receptor desensitization, whereas CNIH-3 acts on deactivation. Because both alternative splicing and TARPs target the AMPAR LBD to regulate desensitization, the flip/flop cassette dominates and acts as a master switch to selectively override TARP-dependent regulation of gating. In contrast, CNIH-3 and CKAMP44 are unaffected by AMPAR alternative splicing. This unique relationship between TARPs and alternative splicing may represent a mechanism by which individual synapses customize their AMPAR responsiveness in a neuronal subtype-specific way. Specific functional properties of the TARP-like auxiliary subunit, GSG1L, are also modified by alternative splicing. Altogether, our study reveals a coordinated effort between alternative RNA splicing and auxiliary protein action to fine-tune AMPAR-mediated signaling in the CNS.

Materials and Methods

Plasmids and molecular biology

All experiments were performed using the rat sequence of the GluA2 subunit with Q/R site unedited i.e., GluA2(Q) in the pRK5 vector. Alternatively spliced isoforms are denoted as flip ($GluA2_i$) or flop ($GluA2_o$). Auxiliary and pore-forming subunits were co-expressed at a 2:1 cDNA ratio (auxiliary in excess), except for mouse TARP γ2 which was in tandem with GluA2 via a short peptide linker (Dawe et al., 2016, 2019). Species and vectors for auxiliary subunits are as follows: human cornichon-3 (CNIH-3) in pCMV-Sport6, mouse GSG1L in pReceiver-M02 (GeneCopoeia), and mouse CKAMP44 in pRK5. Constructs were co-transfected with a plasmid encoding enhanced green fluorescent protein (eGFP) to identify transfected cells.

Cell culture and transfection

HEK293T/17 cells (ATCC) were maintained in MEM supplemented with GlutaMAX and 10% fetal bovine serum (FBS). Cells were plated at low density (1.6×10^4 cells/ml) on poly-D-lysine-coated 35-mm dishes. Transient transfection was completed 48 h post-plating using the calcium phosphate precipitation method. After 6–12 h, cells were washed twice with PBS and maintained in fresh medium including 30 μM NBQX to minimize AMPAR/auxiliary-induced cytotoxicity.

Electrophysiology recordings

Electrophysiological responses were recorded 24–48 h post-transfection from outside-out patches excised from transfected cells. Recording pipettes were composed of borosilicate glass (3–6 MΩ, King Precision Glass) coated with dental wax. All recordings were performed using an Axopatch 200B amplifier (Molecular Devices, LLC). Current records were filtered at 5 or 10 kHz and sampled at 25–50 kHz. Series resistance (3–12 MΩ) was compensated by 95%. The holding potential during recordings was −60 or −100 mV. All experiments were performed at room temperature. Data were acquired using pClamp9 software (Molecular Devices, LLC).

External solution contained (in mM): 150 NaCl, 5 HEPES, 0.1 $CaCl_2$, 0.1 $MgCl_2$, and 2% phenol red, pH 7.3–7.4. Internal solution contained (in mM): 115 NaCl, 10 NaF, 5 HEPES, 5 Na_4BAPTA, 0.5 $CaCl_2$, 1 $MgCl_2$, and 10 Na_2ATP, pH 7.3–7.4. The osmotic pressure of all solutions was adjusted to 295–300 mOsm with sucrose. Concentrated (10×) agonist solution stocks were prepared by dissolving L-Glutamate (L-Glu) directly in external solution. L-Glu was applied at a final concentration of 10 mM using a piezo-stack driven perfusion system (Physik Instrumente). Solution exchange (<400 μs) was determined by measuring the liquid junction current at the end of each experiment.

Data analysis

Electrophysiological data were analyzed using Clampfit 10.5 (Molecular Devices, LLC) and tabulated in Excel. Current decay rates were fit using 1st or 2nd order exponential functions of the form $y = A_i{}^*\exp(-x/\tau_i)$. For decay rates requiring 2nd order exponential fits, time constants are presented using both the individual components and as weighted means. When measuring decay kinetics, all patch recordings were fit by both mono-exponential and bi-exponential functions and the best fit was selected based on visual inspection, the validity of the tau values/contributions, as well as the goodness of fit. To measure recovery from desensitization, a two-pulse protocol was used in which agonist was applied at variable interpulse intervals, and the peak amplitude of the second (test) pulse was expressed as a fraction of the peak amplitude of the first (initial) pulse. Recovery data were fit with both mono-exponential and bi-exponential functions and the best fit (based on ability to converge and R^2 value) was selected to obtain $\tau_{recovery}$. All data were illustrated using Origin 2020 (OriginLab) and Adobe Illustrator CS5.

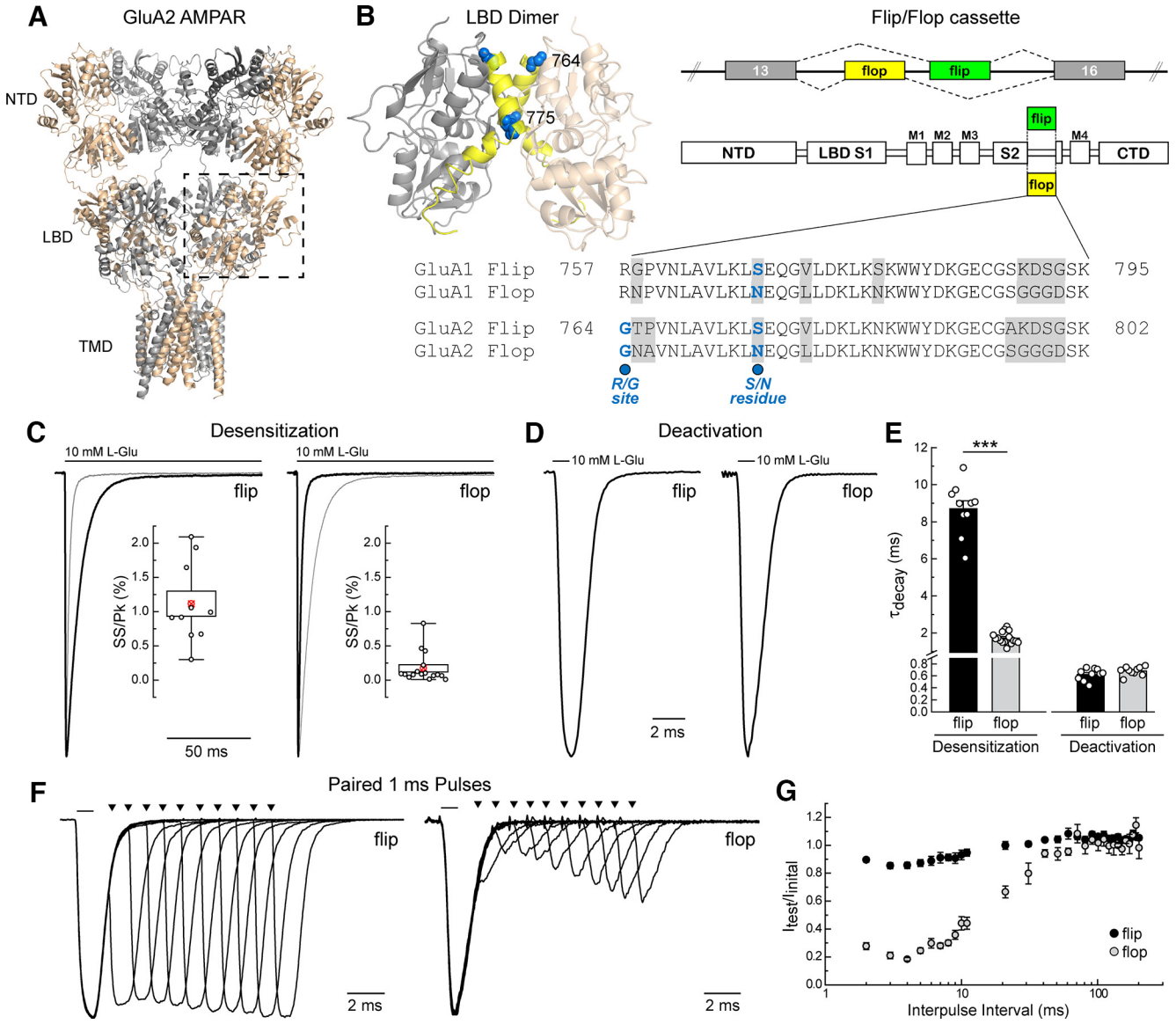

Figure 1. Alternative splicing of GluA2 AMPARs yields flip and flop isoforms with distinct desensitization kinetics. ***A***, Cryo-EM structure of a GluA2 homotetramer (PDB: 5L1B) in the apo state. NTD, amino-terminal domain; LBD, ligand-binding domain; TMD, transmembrane domain. Dashed box emphasizes LBD dimer. ***B***, Left, Structure of isolated GluA2$_o$ LBD dimer (PDB: 6GL4) with residues 764 and 775 shown as blue spheres. The region corresponding to the flip/flop cassette (helices J and K) is colored in yellow. Right, Annotated gene diagram depicting mutually exclusive flop (yellow) and flip (green) exons. The sequence of the flip/flop cassette is shown for GluA1 and GluA2 subunits. Amino acids that differ between splice variants are shaded gray. In GluA2, RNA editing occurs at the R/G site at position 764. The S/N residue at position 768 in GluA1 and 775 in GluA2 is a key molecular determinant of receptor function and allosteric modulation. ***C***, Representative normalized current traces for GluA2 flip (left, patch 180308p6) and flop (right, patch 181015p10) receptors in response to a 250-ms application of 10 mM L-Glu. The gray trace depicts the current response for one GluA2 splice variant in comparison to its counterpart in black. The inset graph shows the steady-state (SS) current amplitude as a percentage of the peak response (Pk). Red circle represents the mean, box represents SEM, whiskers span minimum and maximum values. Data points represent individual patch recordings. ***D***, Representative normalized current traces for GluA2 flip (left, patch 180308p6) and flop (right, patch 181001p9) receptors in response to a 1-ms application of 10 mM L-Glu. ***E***, Weighted time constants of current decay (τ_{decay}) upon 250-ms (desensitization) and 1-ms (deactivation) L-Glu applications for GluA2 flip and flop receptors. Desensitization: $U_{(10,16)} = 160$, $^{***}p < 0.001$, Mann–Whitney *U* test. Deactivation: $t_{(18)} = -1.424$, $p = 0.172$, unpaired two-tailed Student's *t* test. Data are mean ± SEM. Data points represent individual patch recordings. ***F***, Paired 1-ms pulses of 10 mM L-Glu were applied at increasing 1-ms intervals (black triangles) to GluA2 flip (left, patch 170406p5) and flop receptors (right, 170421p4). The first test pulse was provided 2 ms after the initial conditioning pulse. ***G***, Normalized current amplitudes at different time intervals for the paired 1-ms pulse protocol described in ***F***. Data are mean ± SEM, where $n = 6$ for flip and $n = 7$ for flop.

Experimental design and statistical analysis

Statistical details can be found in the figure legends. Data are presented as mean ± SEM, where *n* values represent the number of individual patches. Data points correspond to individual patches for each transfection condition. Transfections were performed at least two independent times. For simple pairwise comparisons, unpaired two-tailed Student's *t* tests (parametric) or Mann–Whitney *U* tests (nonparametric) were conducted as indicated. For datasets involving comparisons between multiple groups, one-way, Kruskal–Wallis, or two-way ANOVAs were performed when appropriate. For one-way ANOVAs, homogeneity of variance was assessed to determine subsequent *post hoc* tests. Tukey's HSD tests (parametric, equal variance), Dunnett's T3 tests (parametric, unequal variance), or Dunn's test (nonparametric) were completed as indicated. Statistical analyses were conducted using SPSS Statistics 24 (IBM) and custom statistical software generously provided by Joe Rochford (McGill University). Significance level was set at 0.05 and is denoted as $^{*}p < 0.05$, $^{**}p < 0.01$, and $^{***}p < 0.001$. Exact *p*-values are provided in the respective figure legends for both significant and nonsignificant results, except when $p < 0.001$.

Table 1. Desensitization kinetics of alternatively spliced GluA2 receptors in the absence and presence of auxiliary subunits

Receptor	Equilibrium response (%)	τ fast (ms)	τ slow (ms)	Contribution of τ fast (%)	τ weighted (ms)	*n*
Alone						
GluA2 flip	1.12 ± 0.18	7.97 ± 0.46	47.1 ± 6.5	96.9 ± 1.1	8.71 ± 0.43	10
GluA2 flop	0.17 ± 0.05	1.57 ± 0.06	14.2 ± 1.3	98.5 ± 0.3	1.73 ± 0.08	16
GluA2 flip						
TARP γ2	22.9 ± 2.4	12.0 ± 0.7	49.1 ± 3.8	72.7 ± 3.6	21.4 ± 1.6	16
CNIH-3	17.8 ± 2.3	18.7 ± 1.1	71.0 ± 5.4	47.8 ± 3.5	47.6 ± 4.5	16
GSG1L	1.80 ± 0.33	7.36 ± 0.30	23.2 ± 1.9	67.9 ± 3.1	12.4 ± 0.9	10
CKAMP44	0.25 ± 0.06	4.76 ± 0.27	16.4 ± 1.3	92.6 ± 1.3	5.55 ± 0.23	8
GluA2 flop						
TARP γ2	3.80 ± 0.66	1.80 ± 0.08	15.2 ± 0.9	94.5 ± 0.7	2.54 ± 0.17	14
CNIH-3	6.13 ± 0.72	6.53 ± 0.35	29.4 ± 2.5	77.0 ± 3.4	11.5 ± 0.8	9
GSG1L	0.37 ± 0.14	1.52 ± 0.22	6.51 ± 1.35	89.8 ± 4.1	1.88 ± 0.15	6
CKAMP44	0.06 ± 0.04	1.08 ± 0.04	3.37 ± 0.33	91.4 ± 1.8	1.25 ± 0.06	6

Equilibrium response refers to the steady-state current as a percentage (%) of the peak response. Weighted time constants (τ weighted) were calculated based on the relative area fit by the fast (τ fast) and slow (τ slow) components. Time constants are listed in milliseconds (ms). The number of patch recordings for each receptor (*n*) is indicated. All values represent mean ± SEM.

Results

Alternative splicing of the flip/flop cassette selectively regulates AMPAR desensitization

To study alternatively spliced AMPAR signaling complexes, we first compared the functional properties of GluA2 flip ($GluA2_i$) and flop ($GluA2_o$) isoforms in the absence of auxiliary subunits. We measured the time course of channel gating in response to long (250 ms) and short (1 ms) applications of 10 mM L-Glu, which provide kinetic information on the rate into macroscopic desensitization (Fig. 1*C*) and deactivation (Fig. 1*D*), respectively.

Consistent with previous work (Mosbacher et al., 1994; Koike et al., 2000; Quirk et al., 2004), each isoform exhibited distinct desensitization kinetics with flop receptors desensitizing 5-fold faster than flip (1.7 ± 0.1 ms, $n = 16$ vs 8.7 ± 0.4 ms, $n = 10$; Fig. 1*C*,*E*; Table 1). Although the steady-state/peak response was relatively small (≤2%) in each case, there was nearly an order of magnitude difference, with flop receptors having more profound equilibrium desensitization than flip receptors (Fig. 1*C*, insets; Table 1). In contrast, the deactivation kinetics of both isoforms were indistinguishable (Fig. 1*D*,*E*), reaffirming that splicing of the flip/flop cassette selectively targets the structural rearrangements that primarily control AMPAR desensitization.

L-glutamic acid (L-Glu) is thought to reside only for brief millisecond periods in the synaptic cleft (Jones and Westbrook, 1996). Accordingly, the kinetics of deactivation, and not desensitization, are thought to be more critical in shaping the time course of synaptic events. Despite this, the flip/flop cassette control over desensitization can still regulate the efficacy of glutamatergic transmission following repetitive channel activations. Figure 1*F* shows typical patch experiments on GluA2 flip and flop isoforms, where the peak responses between conditioning and test agonist pulses were compared at different time intervals. For $GluA2_i$ receptors, the peak amplitude of the test response decreased by only 14.5 ± 2.2% ($n = 6$), demonstrating that a relatively small proportion of AMPARs desensitized during the conditioning pulse. In contrast, most $GluA2_o$ AMPARs desensitized during the conditioning pulse as the peak amplitude of the test response decreased by 81.6 ± 1.3% ($n = 7$) compared with the initial response (Fig. 1*G*). These findings establish that alternative splicing impacts the responsiveness of AMPARs even to brief 1-ms applications of L-Glu, in agreement with the proposal that flop receptors are more prone to desensitize from a closed state (Raman and Trussell, 1995).

We next sought to understand how AMPAR alternative splicing may impact modulation by auxiliary subunits. Our lab has previously shown that alternative splicing affects TARP regulation of desensitization (Dawe et al., 2019), but whether this distinction can be extended to other AMPAR auxiliary protein families, such as CNIHs, has yet to be explored. To investigate this, we compared TARP γ2 and CNIH-3 regulation of AMPAR channel gating (Figs. 2, 3) and then examined the impact of the flip/flop cassette (Figs. 4, 5).

TARP γ2 and CNIH-3 regulate AMPARs by targeting different gating events

TARPs and CNIHs are essential components of native AMPAR complexes (Matthews et al., 2021; Yu et al., 2021). They have largely been assumed to operate through a common allosteric mechanism since they regulate the gating and permeation properties of AMPARs similarly (Hansen et al., 2021). TARPs and CNIHs are, however, structurally dissimilar (Nakagawa, 2019; Kamalova and Nakagawa, 2021) with TARPs possessing two extracellular loops that interact with the AMPAR LBD (Dawe et al., 2016; Twomey et al., 2016; Riva et al., 2017), whereas the CNIH structure is restricted to the plasma membrane and AMPAR TMD (Nakagawa, 2019).

As reported by our lab and others (Priel et al., 2005; Coombs et al., 2012; Brown et al., 2018), the Type I TARP γ2 and CNIH-3 both slow the rate and degree of macroscopic desensitization of $GluA2_i$ AMPARs (Fig. 2*A*; Table 1). Kinetic analysis revealed that desensitization was best fit by the sum of two exponential functions (τ_{fast}, τ_{slow}) with the fast, more dominant component varying according to the presence or absence of auxiliary proteins (Fig. 2*A*,*C*,*E*). The fast decay component (τ_{fast}) for $GluA2_i$ receptors alone was 8.0 ± 0.5 ms ($n = 10$) and represented 96.9% of the overall response (Table 1). Co-assembly with TARP γ2 slowed fast desensitization to 12.0 ± 0.7 ms ($n = 16$) while decreasing its overall contribution to 72.7% (Fig. 2*C*,*E*). Receptor complexes co-assembled with CNIH-3 also exhibited slower desensitization rates, with the fast decay component of 18.7 ± 1.1 ms ($n = 16$) contributing 47.8% to the overall response (Fig. 2*C*,*E*). The slower decay component (τ_{slow}) for $GluA2_i$ receptors alone was 47.1 ± 6.5 ms which contributed only 3.1% to the overall response (Fig. 2*C*). Although TARP γ2 did not alter time constant of the slow component (49.1 ± 3.8 ms), it increased its overall contribution by 13-fold (Fig. 2*C*,*E*; Table 1). By contrast, CNIH-3 significantly prolonged the slow component of desensitization to 71.0 ± 5.4 ms and increased its contribution by 25-fold to 52.2% (Fig. 2*C*,*E*; Table 1). On that note, the steady-state/peak

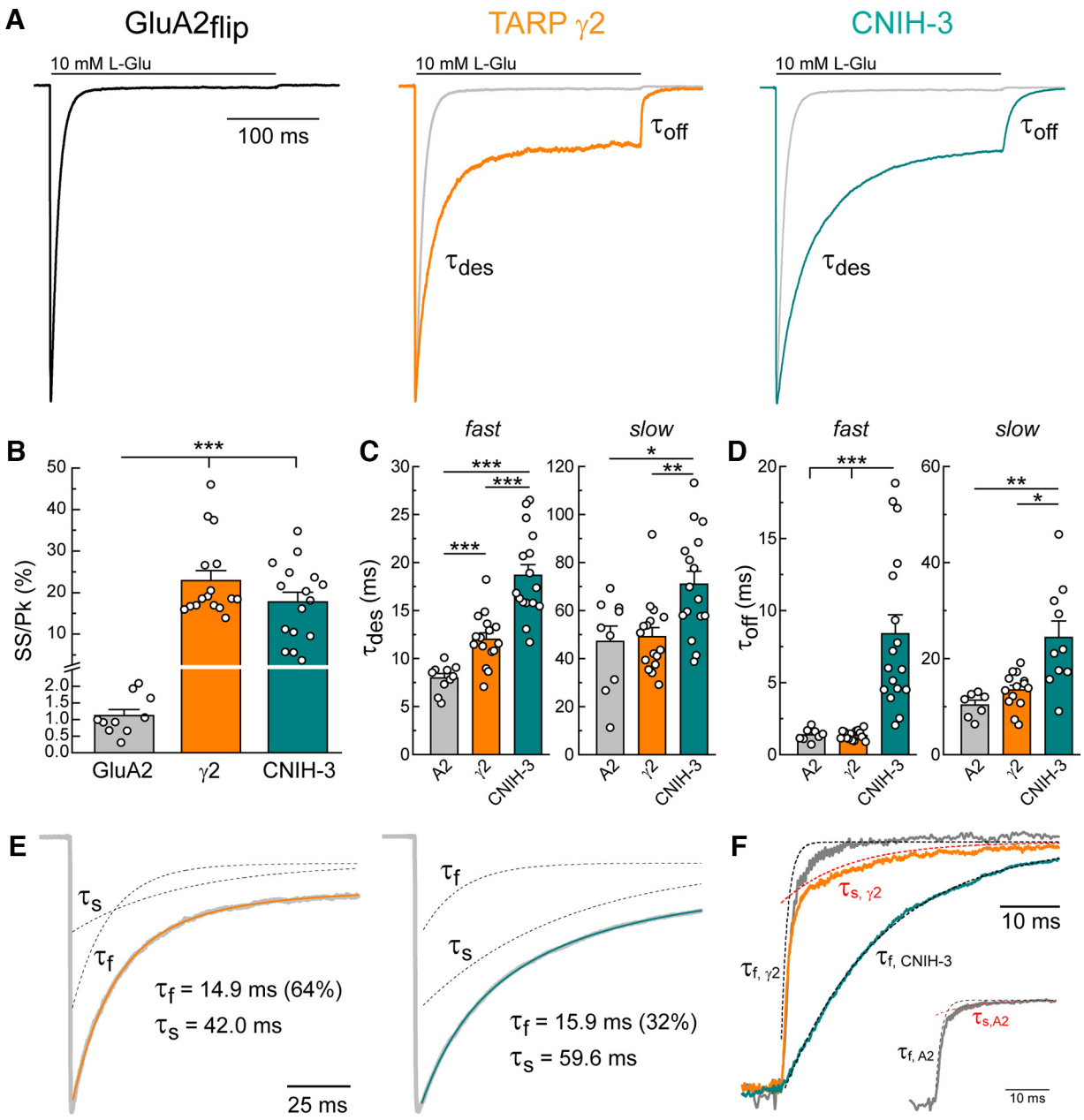

Figure 2. TARP γ2 and CNIH-3 prolong entry into desensitization of GluA2 flip receptors by targeting different gating events. ***A***, Representative normalized current traces for GluA2 flip expressed alone (black, patch 180308p6), with TARP γ2 (orange, patch 180315p2), or with CNIH-3 (cyan, patch 190115p5) in response to a long, 250-ms application of 10 mM L-Glu. ***B***, Steady-state (SS) current amplitude as a percentage of the peak response (Pk). $F_{(2,39)} = 22.00$, $p < 0.001$, one-way ANOVA. Dunnett's T3 test, ***$p < 0.001$, γ2 versus CNIH-3 $p = 0.342$. Data are mean ± SEM. ***C***, Desensitization time constants (τ_{des}) represented by the fast (left) and slow (right) components of current decay. Fast component: $F_{(2,39)} = 34.68$, $p < 0.001$, one-way ANOVA. Dunnett's T3 test, ***$p < 0.001$. Slow component: $F_{(2,38)} = 7.01$, $p = 0.003$, one-way ANOVA. Tukey's HSD test, *$p = 0.012$, ** $p = 0.006$, A2 versus γ2 $p = 0.964$. Of the 10 recordings for GluA2, one was best fit by a mono-exponential function. Data are mean ± SEM. ***D***, Off kinetic time constants (τ_{off}) represented by the fast (left) and slow (right) components of current decay. Fast component: $H_{(2)} = 27.77$, $p < 0.001$, Kruskal–Wallis ANOVA. Dunn's test, ***$p < 0.001$, A2 versus γ2 $p = 0.999$. Slow component: $F_{(2,28)} = 11.05$, $p < 0.001$, one-way ANOVA. Dunnett's T3 test, *$p = 0.033$, **$p = 0.008$, A2 versus γ2 $p = 0.113$. Data are mean ± SEM. For ***B–D***, data points represent individual patch recordings. ***E***, Current traces for AMPAR-auxiliary complexes presented in ***A*** on a shorter time scale showing the individual contribution of the fast (τ_f) and slow (τ_s) components to the overall current decay. Dotted lines represent bi-exponential fit components, colored lines represent weighted fit. ***F***, Overlay of current decay traces upon removal of L-Glu at the end of the 250-ms pulse. Off kinetics of GluA2 (gray and inset) and GluA2-γ2 (orange) receptors must always be fit by two exponentials, whereas off kinetics of GluA2-CNIH-3 (cyan) can be fit by a single exponential function (in some cases).

response increased from 1.1 ± 0.2% ($n = 10$) for $GluA2_i$ alone to 22.9 ± 2.4% ($n = 16$) with γ2 and 17.8 ± 2.3% ($n = 16$) with CNIH-3 (Fig. 2*A*,*B*; Table 1) representing a substantial attenuation of equilibrium desensitization. Taken together, although both TARP γ2 and CNIH-3 attenuate AMPAR macroscopic desensitization, they achieve this by targeting different kinetic states.

In keeping with this, the off kinetics observed following cessation of the agonist application were distinct between TARP γ2- and CNIH-3-bound AMPARs (Fig. 2*A*,*D*,*F*; Table 2). The off kinetics (τ_{off}) could be fit by the sum of two exponentials with the fast and slow components being kinetically indistinguishable between TARP-bound and unbound receptors. For example, the fast component of τ_{off} was 1.3 ± 0.1 ms ($n = 14$) and 1.4 ± 0.2 ms ($n = 8$) for $GluA2_i$ with and without TARPs, respectively (Fig. 2*D*). However, the fast component of τ_{off} contributed less to the response for TARPed receptors (64.0% of response) compared

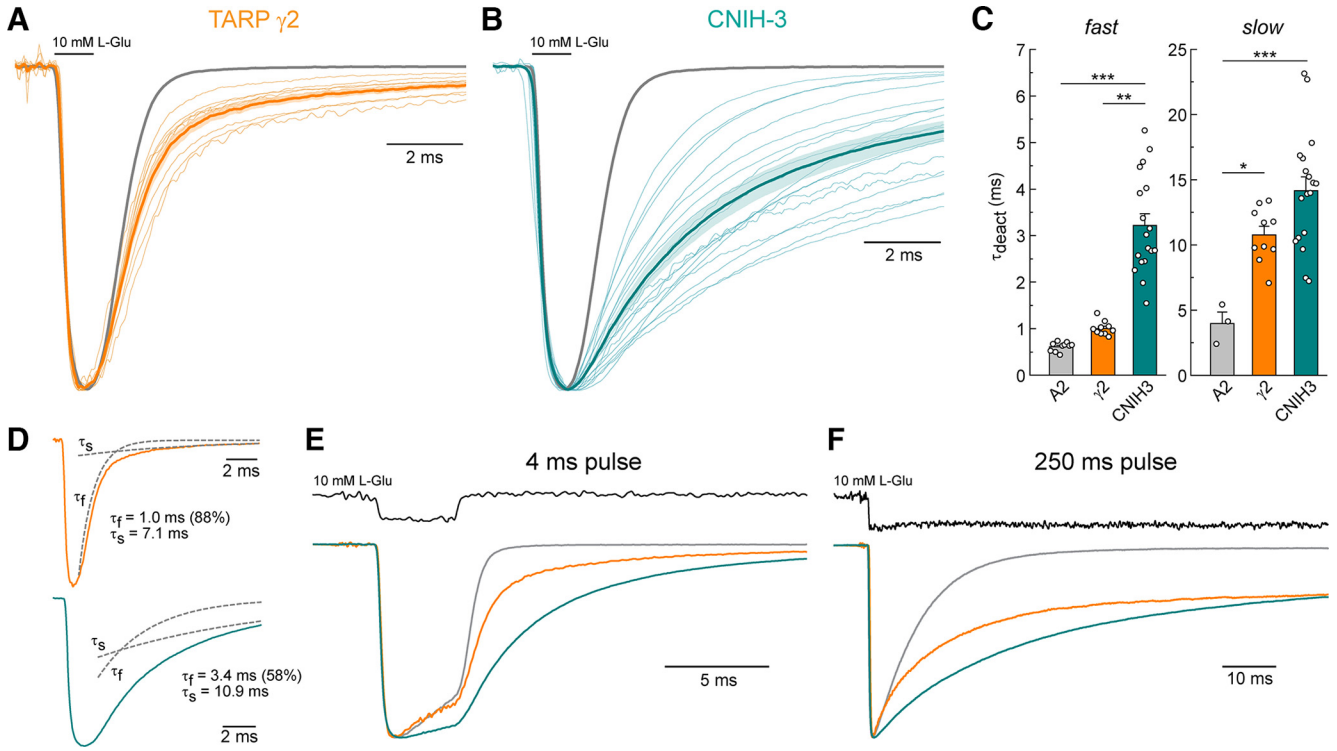

Figure 3. CNIH-3 but not TARP γ2 preferentially prolongs GluA2 flip deactivation. ***A***, ***B***, Normalized current traces for GluA2 flip receptors bound by (***A***) TARP γ2 ($n = 10$ recordings) or (***B***) CNIH-3 ($n = 18$ recordings) in response to brief, 1-ms applications of 10 mM L-Glu. The thick orange and cyan lines depict the averaged deactivation response for AMPARs bound by TARP γ2 and CNIH-3, respectively, and the shaded area represents the SEM. The solid gray trace in both panels represents the averaged deactivation response for GluA2 flip receptors alone from $n = 10$ individual patch experiments. ***C***, Deactivation time constants (τ_{deact}) represented by the fast (left) and slow (right) components of current decay. Of the 10 recordings for GluA2, seven were best fit by a mono-exponential function. Fast component: $H_{(2)} = 31.74$, $p < 0.001$, Kruskal–Wallis ANOVA. Dunn's test, $^{**}p = 0.004$, $^{***}p < 0.001$, A2 versus γ2 $p = 0.133$. Slow component: $F_{(2,28)} = 10.80$, $p < 0.001$, one-way ANOVA. Tukey's HSD test, $^{*}p = 0.024$, $^{***}p < 0.001$, γ2 versus CNIH-3 $p = 0.067$. Data are mean ± SEM. Data points represent individual patch recordings. ***D***, Representative normalized current traces for GluA2 flip expressed with TARP γ2 (top, patch 190115p9) or with CNIH-3 (bottom, patch 190115p5) depicting the fast (τ_f) and slow (τ_s) components of deactivation and their percent contribution to the overall current decay. ***E***, ***F***, Scaled current responses of GluA2 flip receptors expressed alone (gray), with TARP γ2 (orange) or with CNIH-3 (cyan) in response to a (***E***) 4-ms or (***F***) 250-ms application of 10 mM L-Glu. Traces are averaged from four to five individual patch experiments. The uppermost trace shows the junction current used to monitor solution exchange rate.

with $GluA2_i$ alone (92.5% of response; Fig. 2*F*). In contrast, the off kinetics of CNIH-3-bound AMPARs were required, in some cases, to be fit by a single exponential and were markedly slower than TARP-bound receptors (Fig. 2*F*). When fit by a single exponential, τ_{off} was slowed to 12.9 ± 2.1 ms ($n = 7$; Fig. 2*F*; Table 2). When fit by two exponentials, both the fast and slow components of τ_{off} were significantly slowed by CNIH-3 compared to $GluA2_i$ with and without γ2, with values of 5.2 ± 0.7 ms (53.9% of response) and 24.4 ± 3.4 ms ($n = 10$), respectively (Fig. 2*D*; Table 2). Why some of our data (seven out of 17 patches) were better fit by a single exponential function is still not clear. Given these distinctions, we reasoned that TARP γ2 and CNIH-3 may target different aspects of AMPAR gating. To examine this further, we studied the impact of both auxiliary proteins on the kinetics of channel closure or deactivation.

CNIH-3 but not TARP γ2 preferentially prolongs AMPAR channel closure

$GluA2_i$ deactivation kinetics were estimated by measuring the decay observed following a brief, 1-ms application of L-Glu (Fig. 3*A–C*; Table 2). $GluA2_i$ receptors activate and inactivate rapidly, where the fast time constant of 0.61 ± 0.03 ms ($n = 10$) represents nearly 100% of the overall current decay (Fig. 3*C*; Table 2). When expressed with TARP γ2, estimates of the fast component were modestly slower than for $GluA2_i$ alone, although not statistically significant (1.0 ± 0.1 ms, $n = 10$; Fig. 3*A*,*C*,*D*). In striking contrast to γ2, CNIH-3 significantly slowed the dominant fast component of $GluA2_i$ deactivation by 5-fold to 3.2 ± 0.3 ms ($n = 18$; Fig. 3*B–D*). This modulation of the fast component by CNIH-3 was indeed more prominent than any effect of TARP γ2 (Fig. 3*C*).

Although the slow component of deactivation contributed <1% to the overall current decay in $GluA2_i$ receptors alone, association with either γ2 or CNIH-3 enhanced this kinetic component, albeit with obvious differences in magnitude (Fig. 3*D*). While γ2 increased the slow component of $GluA2_i$ deactivation from 4.0 ± 0.9 ms ($n = 3$) to 10.8 ± 0.6 ms ($n = 10$), the slow component contributed only ~10% to the overall response (Fig. 3*C*, *D*; Table 2). Conversely, CNIH-3 slowed the slow component by 3.5-fold to 14.2 ± 1.0 ms ($n = 18$), while substantially increasing its proportion to over 30% of the overall response (Fig. 3*C*,*D*; Table 2). These data demonstrate that γ2 has only a minor effect on channel closure, whereas the primary effect of CNIH-3 is to slow deactivation.

Extending these observations further, when the length of the agonist application was varied to an intermediate (4 ms) or a long (250 ms) duration to allow the onset of desensitization, TARPs and CNIHs again differentially modified the $GluA2_i$ current decay profile (Fig. 3*E*,*F*). Most interestingly, for intermediate (4 ms) L-Glu applications, the CNIH-3-bound $GluA2_i$ receptor current decay was slower compared with $GluA2_i$ alone, both in the sustained presence of agonist and following agonist removal,

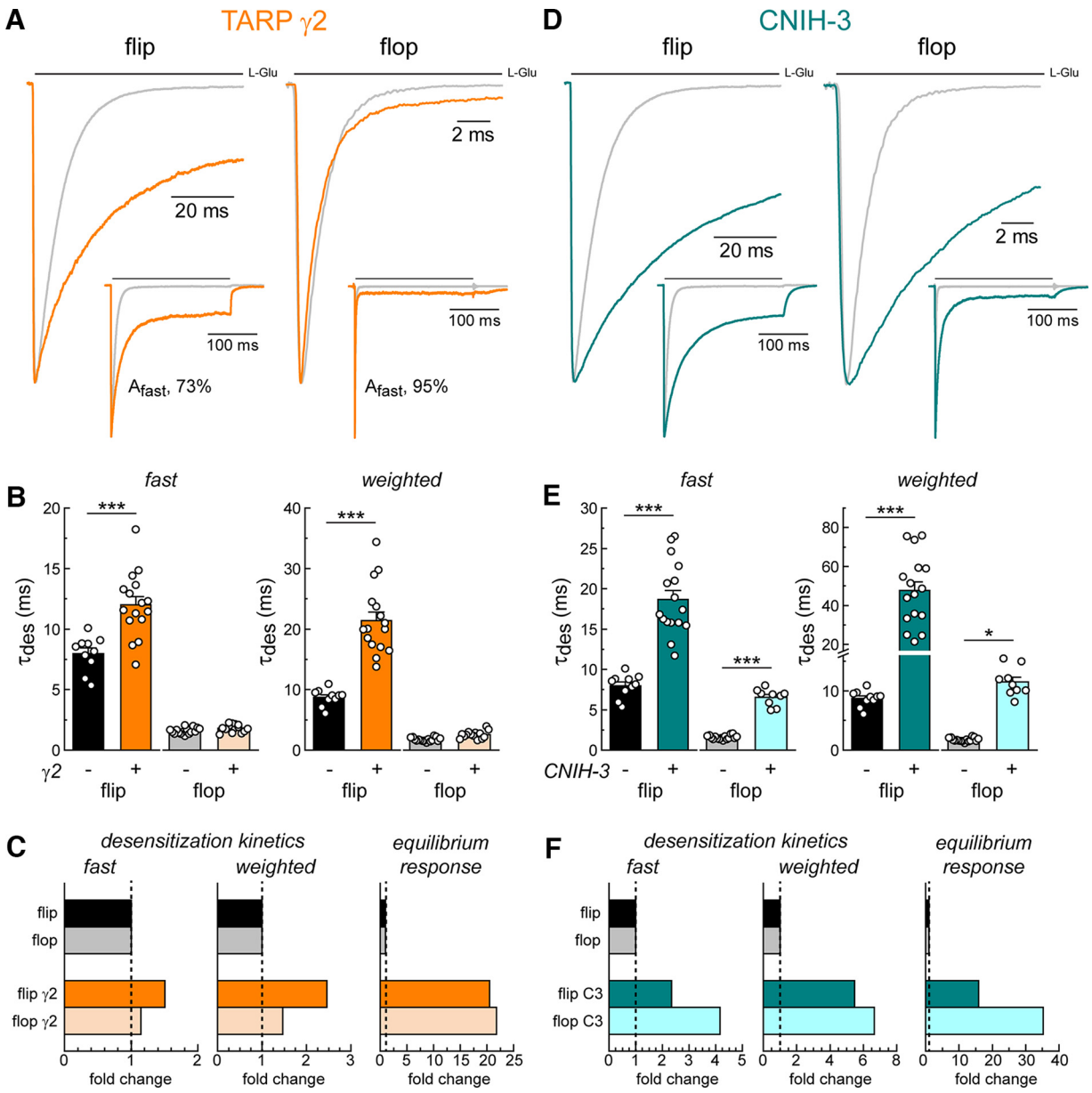

Figure 4. Alternative splicing overrides TARP γ2, but not CNIH-3, slowing of desensitization. ***A***, Representative normalized current traces for GluA2 flip (left, patch 180315p2) and flop (right, patch 170424p3) receptors expressed with TARP γ2 in response to a 250-ms application of 10 mM L-Glu. The gray traces depict the current response of GluA2 receptors in the absence of TARPs. Insets show the full current decay on a longer time scale and indicate the percent contribution of the fast component of desensitization to the overall current decay (A_{fast}). ***B***, Desensitization time constants (τ_{des}) for the fast component of current decay (left) and weighted response (right). Fast component: Interaction, $F_{(1,52)} = 19.84$, $p < 0.001$; flip ± γ2, $F_{(1,52)} = 40.60$, ***$p < 0.001$; flop ± γ2, $F_{(1,52)} = 0.15$, $p = 0.696$. Weighted: Interaction, $F_{(1,52)} = 49.01$, $p < 0.001$; flip ± γ2, $F_{(1,52)} = 102.01$, ***$p < 0.001$; flop ± γ2, $F_{(1,52)} = 0.50$, $p = 0.481$. Two-way ANOVA with Simple Main Effects test for auxiliary at splice variant. Data are mean ± SEM. ***C***, Fold change summary for fast and weighted time constants of desensitization, as well as the equilibrium response for flip and flop GluA2 receptors expressed with TARP γ2. ***D***, Representative normalized current traces for GluA2 flip (left, patch 190115p5) and flop (right, patch 181012p3) receptors expressed with CNIH-3 in response to a 250-ms application of 10 mM L-Glu. The gray traces depict the current response of GluA2 receptors in the absence of CNIHs. Insets show the full current decay on a longer time scale. ***E***, Desensitization time constants (τ_{des}) for the fast component of current decay (left) and weighted response (right). Fast component: Interaction, $F_{(1,47)} = 13.76$, $p < 0.001$; flip ± CNIH-3, $F_{(1,47)} = 99.09$, ***$p < 0.001$; flop ± CNIH-3, $F_{(1,47)} = 19.98$, ***$p < 0.001$. Weighted: Interaction, $F_{(1,47)} = 24.16$, $p < 0.001$; flip ± CNIH-3, $F_{(1,47)} = 89.11$, ***$p < 0.001$; flop ± CNIH-3, $F_{(1,47)} = 5.26$, *$p = 0.026$. Two-way ANOVA with Simple Main Effects test for auxiliary at splice variant. Data are mean ± SEM. For ***B***, ***E***, data points represent individual patch recordings. ***F***, Fold change summary for fast and weighted time constants of desensitization, as well as the equilibrium response for flip and flop GluA2 receptors expressed with CNIH-3 (C3).

consistent with CNIH-3 targeting the fast component of current decay. In contrast, TARP γ2-bound receptor current decay more closely resembled that of $GluA2_i$ alone in the presence of the agonist (Fig. 3*E*).

Together from these observations, we propose that TARPs and CNIHs regulate AMPARs by targeting distinct gating events. Our findings suggest that TARPs primarily act on the process of desensitization; on the contrary, CNIH-3 modulation primarily affects deactivation from the outset of current decay. Structurally, this distinction could be explained by the large extracellular region of TARPs which stabilizes the AMPAR LBD to prolong desensitization (Dawe et al., 2016; Twomey et al., 2016), whereas CNIHs act exclusively in the membrane at the level of the ion channel pore and are thus primed to slow deactivation/channel closure (Nakagawa, 2019). Because the two gating processes are coupled (Partin et al., 1996), TARPs and

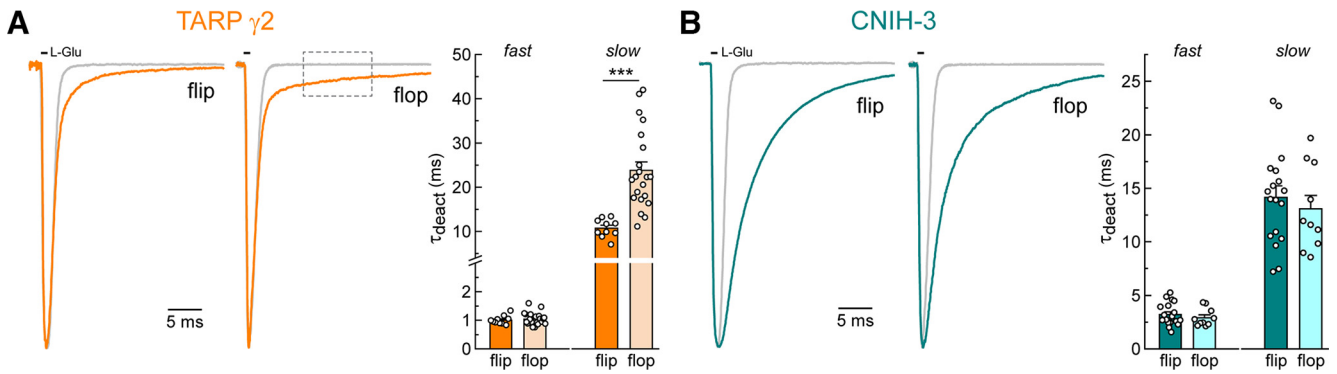

Figure 5. CNIH-3 modulation of channel closure is independent of alternative splicing. ***A***, Representative normalized current traces for GluA2 flip (left) and flop (middle) expressed with TARP γ2. Bar graph (right) shows deactivation time constants (τ_{deact}) represented by the fast and slow components of current decay for TARP-bound receptors. Fast component: $t_{(29)} = -0.478$, $p = 0.636$, unpaired two-tailed Student's *t* test. Slow component: $U_{(10,21)} = 203$, $^{***}p < 0.001$, Mann–Whitney *U* test. Data are mean ± SEM. ***B***, Representative normalized current traces for GluA2 flip (left) and flop (middle) expressed with CNIH-3. Bar graph (right) shows deactivation time constants (τ_{deact}) represented by the fast and slow components of current decay for CNIH-3-bound receptors. Fast component: $U_{(18,10)} = 107$, $p = 0.436$, Mann–Whitney *U* test. Slow component: $t_{(26)} = 0.642$, $p = 0.527$, unpaired two-tailed Student's *t* test. Data are mean ± SEM. For ***A***, ***B***, data points on bar graphs represent individual patch recordings.

Table 2. Off and deactivation kinetics of alternatively spliced GluA2 receptors in the absence and presence of auxiliary subunits

Receptor	τ fast (ms)	τ slow (ms)	Contribution of τ fast (%)	τ weighted (ms)	*n*
Off kinetics					
GluA2 flip	1.37 ± 0.15	10.3 ± 1.0	92.5 ± 2.2	1.96 ± 0.17	8
TARP γ2	1.34 ± 0.09	13.4 ± 1.0	64.0 ± 3.5	5.89 ± 0.62	14
CNIH-3 (pooled)	8.38 ± 1.32	24.4 ± 3.4	72.9 ± 6.2	13.7 ± 1.6	17
CNIH-3 (bi)	5.23 ± 0.73	24.4 ± 3.4	53.9 ± 4.2	14.2 ± 2.3	10
CNIH-3 (mono)	12.9 ± 2.1	–	100 ± 0	12.9 ± 2.1	7
Deactivation					
Alone					
GluA2 flip (pooled)	0.61 ± 0.03	3.98 ± 0.87	99.6 ± 0.2	0.63 ± 0.03	10
GluA2 flip (bi)	0.59 ± 0.05	3.98 ± 0.87	98.8 ± 0.5	0.60 ± 0.07	3
GluA2 flip (mono)	0.64 ± 0.04	–	100 ± 0	0.64 ± 0.04	7
GluA2 flop	0.68 ± 0.02	–	100 ± 0	0.68 ± 0.02	10
TARP γ2					
GluA2 flip	1.00 ± 0.05	10.8 ± 0.6	87.5 ± 1.3	2.23 ± 0.19	10
GluA2 flop	1.04 ± 0.05	23.8 ± 2.0	91.9 ± 1.2	3.03 ± 0.42	21
CNIH-3					
GluA2 flip	3.22 ± 0.25	14.2 ± 1.0	67.0 ± 5.5	7.08 ± 0.94	18
GluA2 flop	2.91 ± 0.26	13.1 ± 1.3	74.4 ± 4.4	5.22 ± 0.47	10

Weighted time constants (τ weighted) were calculated based on the relative area fit by the fast (τ fast) and slow (τ slow) components. Time constants are listed in milliseconds (ms). The "off kinetics" were calculated from an exponential fit of the decay from the steady-state current after removal of glutamate (i.e., the current decay at the end of a 250-ms application of L-Glu). In some cases, current decay was best fit by a mono-exponential function, as indicated (see Materials and Methods). The number of patch recordings for each receptor (*n*) is indicated. All values represent mean ± SEM.

CNIHs also have indirect effects on deactivation and desensitization, respectively. Based on these assumptions, a modification to the core AMPAR that selectively targets one gating process, such as alternative splicing which targets desensitization, should be able to delineate TARP γ2 from CNIH-3 modulation. Indeed, we have previously shown that flop overrides TARP regulation of AMPAR desensitization (Dawe et al., 2019), but its effect on CNIH regulation has yet to be explored.

Alternative splicing overrides TARP γ2-but not CNIH-3-mediated effects on AMPARs

To test the hypothesis that TARPs and CNIHs target distinct gating events, we examined the effect of alternative splicing on TARP γ2 and CNIH-3 modulation by comparing their ability to regulate flop variants of GluA2 (Fig. 4). As we observed previously, unlike flip receptors, the ability of TARP γ2 to attenuate entry into desensitization of flop receptors was almost completely eliminated (Fig. 4*A*, right; Dawe et al., 2019). The fast and weighted time constants of desensitization for $GluA2_o$-γ2 receptors were similar to flop receptors alone, with the fast component dominating the overall response (1.8 ± 0.1 ms, 94.5% of response, $n = 14$; Fig. 4*B*,*C*; Table 1). Although the degree of equilibrium desensitization was smaller for $GluA2_o$-γ2 receptors (3.8 ± 0.7%) compared with $GluA2_i$-γ2 receptors (22.9 ± 2.4%; Fig. 4*A*, insets; Table 1), the fold changes compared with their respective controls were similar (Fig. 4*C*). Much of this effect can be explained by the difference in equilibrium desensitization observed between GluA2 flip and flop receptors alone (Fig. 1*C*).

In marked contrast to TARP γ2, alternative splicing of GluA2 had no effect on the modulatory capacity of CNIH-3 (Fig. 4*D*). CNIH-3 significantly delayed the onset of $GluA2_o$ desensitization, slowing the fast and more dominant time constant by 4-fold from 1.6 ± 0.1 ms (98.5% of response, $n = 16$) to 6.5 ± 0.4 ms (77.0% of response, $n = 9$; Fig. 4*E*,*F*; Table 1). Again, although the degree of equilibrium desensitization was smaller for CNIH-3-bound flop receptors compared with flip receptors (6.1 ± 0.7% vs 17.8 ± 2.3%; Fig. 4*D*, insets; Table 1), it still represented an increase in the steady-state/peak response by over 30-fold relative to unbound $GluA2_o$ receptors (Fig. 4*F*). Together, our data demonstrate that alternative splicing of the flip/flop cassette selectively controls AMPAR desensitization, which in turn selectively attenuates TARP γ2-mediated slowing of rates into desensitization. Since CNIH-3 does not directly regulate desensitization, CNIH-3 modulation of AMPARs is not impacted by alternative splicing.

CNIH-3 modulation of channel closure is also independent of alternative splicing

We next investigated the effect of alternative splicing on TARP γ2 and CNIH-3 modulation of flop receptor deactivation (Fig. 5). Since the time course of deactivation is similar between GluA2 flip and flop receptors alone (Fig. 1*D*,*E*), any effect of TARP γ2 or CNIH-3 on this gating process was not expected to be affected by alternative splicing. In keeping with this, the negligible effect of TARP γ2 on the dominant fast component of $GluA2_i$ receptor deactivation was statistically indistinguishable

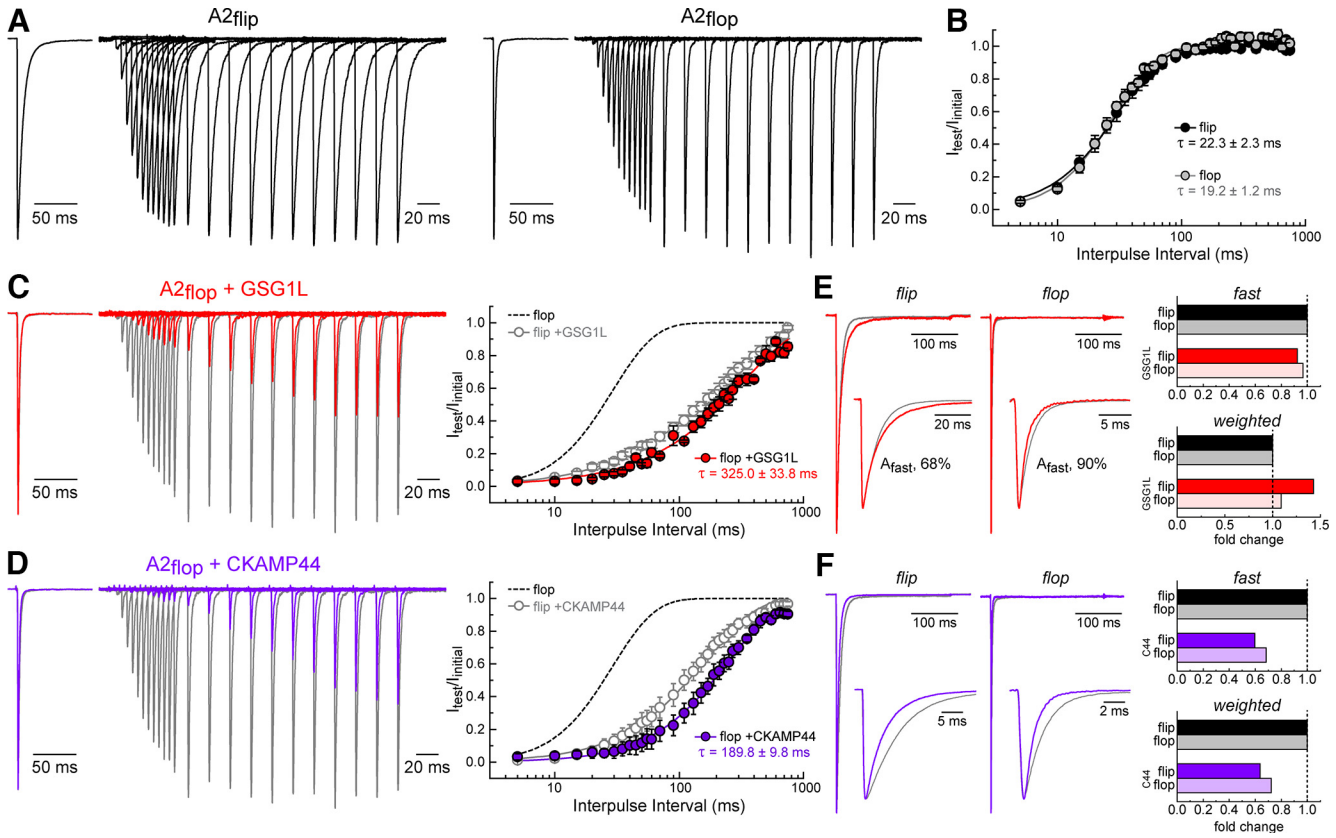

Figure 6. The flip/flop cassette has no effect on the slowing of recovery from desensitization by GSG1L and CKAMP44. ***A***, Recovery from desensitization for GluA2 flip (left) and flop (right) receptors. Recovery was probed using a paired pulse protocol with a conditioning agonist application (250 ms, 10 mM L-Glu) to induce receptor desensitization, which was followed by a test pulse at varying time intervals. Current traces are normalized to the initial response. ***B***, Normalized current amplitudes at different time intervals map the time course of recovery from desensitization. The solid lines represent average fits and the corresponding recovery time constants (τ) are shown. Data are mean ± SEM where $n = 7$ for flip and $n = 16$ for flop. ***C***, Recovery from desensitization for GluA2 flop receptors expressed with GSG1L, as described in ***A***. Plot on the right depicts normalized current amplitudes at different time intervals. The lines represent average fits for GluA2 flop alone (dashed black), GluA2 flip with GSG1L (gray) and GluA2 flop with GSG1L (red). Data points are mean ± SEM where $n = 6$ (flip) and $n = 4$ (flop). ***D***, Recovery from desensitization for GluA2 flop receptors expressed with CKAMP44, as described in ***A***. Plot on the right depicts normalized current amplitudes at different time intervals. The lines represent average fits for GluA2 flop alone (dashed black), GluA2 flip with CKAMP44 (gray) and GluA2 flop with CKAMP44 (purple). Data points are mean ± SEM where $n = 5$ (flip) and $n = 7$ (flop). ***E***, Desensitization kinetics for GluA2 flip and flop receptors expressed with GSG1L. Representative traces are normalized to the peak response; insets depict the percent contribution of the fast component of desensitization to the overall current decay (A_{fast}) and show decay on a shorter time scale. Patch numbers (red traces): flip, patch 180806p5; flop, patch 181018p1.The column charts on the right indicate the fold change summary for the fast and weighted time constants of desensitization. ***F***, Desensitization kinetics for GluA2 flip and flop receptors expressed with CKAMP44. Representative traces are normalized to the peak response; insets depict the current decay on a shorter time scale. Patch numbers (purple traces): flip, 180507p3; flop, 181029p1. The column charts on the right indicate the fold change summary for the fast and weighted time constants of desensitization.

from GluA2$_o$ receptors (Fig. 5*A*; Table 2). Unexpectedly, however, TARP γ2 significantly delayed the time constant for the slow component of deactivation from 10.8 ± 0.6 ms ($n = 10$) for GluA2$_i$ to 23.8 ± 2.0 ms ($n = 21$) for GluA2$_o$ (Fig. 5*A*, see dashed box). A possible explanation for the significantly enhanced slow component of deactivation imparted by TARP γ2 is that this slow component corresponds to receptors desensitizing from the closed state, the proportion of which is much greater for flop receptors (Fig. 1*F*). Since we have shown that TARP γ2 primarily acts to attenuate the process of desensitization (Figs. 2, 3), this component of GluA2$_o$ receptor deactivation (which is really the accumulation of desensitization within a short pulse) is regulated by TARP γ2.

In contrast to TARP γ2, CNIH-3 behaved predictably, slowing both the fast and slow components of deactivation of flop receptors to the same degree as flip receptors (Fig. 5*B*). For example, the fast and dominant time constant of deactivation was increased from 0.68 ± 0.02 ms (100% of response, $n = 10$) for GluA2$_o$ alone compared with 2.9 ± 0.3 ms (74.4% of response, $n = 10$) in the presence of CNIH-3, corresponding to a 4-fold slowing of channel closure (Fig. 5*B*; Table 2).

Alternative splicing does not affect recovery from AMPAR desensitization with or without GSG1L or CKAMP44

In addition to TARP γ2 and CNIH-3, other prominent AMPAR auxiliary proteins include GSG1L and CKAMP44 (von Engelhardt et al., 2010; Shanks et al., 2012). GSG1L is evolutionarily-related and structurally similar to TARPs; in fact, they belong to the same superfamily of claudin proteins (Twomey et al., 2019). Paradoxically, GSG1L and TARPs impart distinct modulatory effects on AMPARs. GSG1L slows rates into desensitization to a lesser degree than TARPs, but more importantly, profoundly slows recovery out of desensitization (Schwenk et al., 2012; Shanks et al., 2012; McGee et al., 2015). Given this, we investigated whether modulation of AMPARs by GSG1L is affected by alternative splicing. For comparison, we additionally studied CKAMP44 which, despite being structurally dissimilar, shares with GSG1L the property of slowing AMPAR recovery from desensitization (von Engelhardt et al., 2010).

We first measured the time course of recovery from desensitization for GluA2 flip and flop receptors alone using a two-pulse protocol (250 ms) separated by increasing time intervals (Fig. 6*A*). Alternative splicing of the flip/flop cassette had no effect on

the recovery process, resulting in recovery time constants of 22.3 ± 2.3 ms ($n = 7$) and 19.2 ± 1.2 ms ($n = 16$) for GluA2 flip and flop isoforms, respectively (Fig. 6*B*; Dawe et al., 2019). Consequently, we predicted that alternative splicing of the flip/flop cassette would not impact canonical modulation by GSG1L and CKAMP44, which is to slow recovery from desensitization. In keeping with this, co-expression of GSG1L with flip and flop receptors resulted in a slowing of recovery kinetics by over 10-fold, to 249.3 ± 28.2 ms ($n = 6$) and 325.0 ± 33.8 ms ($n = 4$), respectively (Fig. 6*C*). Likewise, CKAMP44 regulated the recovery time course of flip (145.4 ± 26.6, $n = 5$) and flop (189.8 ± 9.8 ms, $n = 7$) receptors similarly, slowing the recovery kinetics by an order of magnitude in each case (Fig. 6*D*).

Interestingly, alternative splicing negatively regulated the modest slowing of AMPAR entry into desensitization by GSG1L, while leaving CKAMP44 modulation intact (Fig. 6*E*,*F*). More specifically, the contribution of the fast component of desensitization for GSG1L-bound receptors increased from 67.9% (flip) to 89.8% (flop), resulting in an overall speeding of desensitization kinetics (Fig. 6*E*, insets; Table 1). In contrast, CKAMP44 retained its ability to further speed up entry into desensitization of rapidly-desensitizing flop receptors to a similar degree as flip receptors (Fig. 6*F*). This additive effect suggests that the mechanisms by which CKAMP44 and flop splice variants favor desensitization must be different.

Taken together, these data reveal two important findings. First, entry into and exit out from AMPAR desensitization can be independently modified by alternative splicing and distinct auxiliary protein families. Second, alternative splicing of the flip/flop cassette selectively controls claudin-like regulation of entry into desensitization, targeting TARP γ2 and GSG1L. Modulation by other auxiliary proteins like CNIH-3 and CKAMP44 are unaffected. From a structural perspective, this distinction could be explained by the large extracellular domains of TARPs and GSG1L which transiently engage with the base of the AMPAR LBD. Since rapid rearrangements of the AMPAR LBD largely dictate desensitization (Sun et al., 2002), alternative splicing may disrupt specific functional interactions between AMPARs and TARPs/GSG1L via its impact on LBD stability and intrinsic receptor mobility (Partin et al., 1996; Quirk et al., 2004; Twomey et al., 2017; Dawe et al., 2019). Since recovery from desensitization likely involves larger-scale, slower conformational rearrangements, this gating property is unaffected by alternative splicing.

Discussion

The present study advances our understanding of alternatively-spliced AMPAR signaling complexes in several important ways. First, we establish that two prominent auxiliary subunits, TARP γ2 and CNIH-3, target different gating modalities of the AMPAR. TARP γ2 primarily acts to attenuate the process of desensitization, while CNIH-3 prolongs channel closure/deactivation. Second, this inherent distinction in turn predetermines TARP γ2 and CNIH-3 sensitivity to regulation by alternative splicing of the AMPAR LBD. Alternative splicing of the flip/flop cassette overrides TARP γ2 modulation of gating while having no effect on CNIH-3, which can be explained by the fact that alternative splicing, like TARP modulation, selectively targets desensitization. Third, alternative splicing does not impact the time course of recovery from desensitization, further supporting the idea that the structural events contributing to entry into and exit out from desensitization must be distinct. Consistent with this, regulation by AMPAR auxiliary subunits known to slow the recovery time course, namely GSG1L and CKAMP44, occurs in a splice variant-independent manner.

Auxiliary subunits target different gating modalities of the AMPA receptor

It is generally accepted that TARPs and CNIHs similarly modify AMPAR function by slowing the time course of macroscopic channel gating (Shi et al., 2010; Coombs et al., 2012); however, recent structural work indicates that the structural basis must be different (Nakagawa, 2019). Here, our data suggest that TARP γ2 selectively and directly targets AMPAR desensitization. Kinetic analysis demonstrates that TARP γ2 prolongs long, desensitizing agonist application responses of AMPARs (Fig. 2) while having only modest effects on the response to brief, deactivating agonist pulses (Fig. 3). TARP γ2 tends to shift the relative contributions of the components of current decay rather than alter the individual time constants, most notably that of the slow component which likely reflects desensitization. In keeping with this, our lab has previously shown that AMPAR desensitization is mediated by the rupture of an intersubunit electrostatic bridge at the LBD apex (Dawe et al., 2016). TARP γ2 stabilizes the base of the LBD dimer via interactions with the KGK motif, interfering with the rearrangements associated with desensitization (Sun et al., 2002; Meyerson et al., 2014), which in turn prolongs the duration of gating (Chen et al., 2017). Our findings are consistent with the proposed TARP-associated modal gating, where individual receptors transition between low-P_{open} and high-P_{open} gating modes, reflecting the fast and slow components in bi-exponential macroscopic current decay, respectively (W. Zhang et al., 2014; Howe, 2015).

Although CNIH-3 slows rates into desensitization, we concluded that it achieves this modulatory effect primarily by slowing the time course of channel closure/deactivation. We reasoned that CNIH-3 does not directly regulate receptor desensitization, which agrees with the fact that its allosteric effects on AMPARs are insensitive to alternative splicing (Figs. 4, 5). This conclusion makes sense from a structural perspective since CNIHs lack an extracellular domain and are thus unlikely to contact the LBD (Nakagawa, 2019). In fact, the primary protein-protein interfaces lie within the membrane at the level of the AMPAR transmembrane domain as well as the cytoplasm (Nakagawa, 2019). The slowing of desensitization observed with CNIHs can therefore be explained if there is coupling between deactivation and desensitization. Indeed, others have observed that these processes are linked (Partin et al., 1996; Trussell, 1998). Given this, the most parsimonious explanation is that CNIHs indirectly prolong desensitization by a coupling mechanism whereby deactivation and desensitization proceed in a sequential manner, with deactivation occurring before desensitization. TARPs thus hinder desensitization with little effect on deactivation, while CNIHs slow deactivation which in turn slows desensitization. Three critical transmembrane residues, C528, L789, and A793, have been identified to mediate CNIH stable association and modulation of AMPAR gating (Hawken et al., 2017). These residues are proposed to interact with three bulky phenylalanine residues unique to CNIHs, which may account for differential gating between TARPs and CNIHs (Nakagawa, 2019). In addition, the lipid geometry in the transmembrane region of AMPAR-auxiliary complexes differs

between TARPs and CNIHs; whether this contributes to functional differences remains to be fully explored (Nakagawa, 2019; D. Zhang et al., 2021). Overall, we propose that TARPs are more likely to modulate AMPARs through a concerted contribution of extracellular and transmembrane components to primarily affect the process of desensitization. On the other hand, since CNIHs act exclusively at the level of TMD interactions, we conclude that they primarily modulate the process of channel closure/deactivation.

A privileged relationship between TARPs and AMPAR alternative splicing

Previous work from our lab has reported that flip and flop receptors exhibit distinct movements at rest, where flop receptors are significantly more mobile than flip receptors. This intrinsic mobility difference predisposes flip and flop receptors to respond differently to neurotransmitter, allosteric anions, and TARP $\gamma2$ auxiliary subunits (Dawe et al., 2019). Rapid desensitization of the flop isoform overrides TARP-mediated slowing of desensitization, such that flop receptors are relatively insensitive to TARPs. Here, we shed new light on this observation by demonstrating that TARP $\gamma2$ action on flip and flop differs because TARPs and alternative splicing both target the same gating process in opposing ways, but flop regulation dominates (Fig. 4). In contrast, we show for the first time that CNIH-3 modulation is insensitive to alternative splicing since CNIHs profoundly slow the time course of deactivation, which remains unaffected by splicing. CNIH-3 targets both the fast and slow components of flop receptor deactivation and, in turn, attenuates flop desensitization kinetics (Figs. 4, 5).

In this study, we also report that alternative splicing modifies rates into but not exit out from desensitization, indicating that these are separable processes (Fig. 6; see also Dawe et al., 2019). Therefore, we predicted that auxiliary proteins which primarily function to modify recovery from desensitization, such as GSG1L and CKAMP44, would be unaffected by alternative splicing. Indeed, we observed that both GSG1L and CKAMP44 dramatically slowed the time course of recovery from desensitization of GluA2 flop receptors similarly to flip receptors. GSG1L is particularly interesting, as it is evolutionarily and structurally related to the TARP family and similarly slows entry into desensitization; however, TARP $\gamma2$ and GSG1L have distinct effects on recovery (Twomey et al., 2017). Worthy to note, the modest slowing of entry into desensitization by GSG1L seen in GluA2 flip receptors is similarly abolished as with TARPs in flop receptors, providing further support for the inability of TARP/GSG1L structural elements to stably engage with flop isoform LBDs. This suggests that TARPs and GSG1L slow entry into desensitization through a common set of structural interactions, likely mediated by their extracellular loops. Whether allosteric coupling exists between alternative splicing and other TARP or CNIH isoforms is an interesting avenue for future study, although we predict that functionally similar Type I TARPs $\gamma3$, $\gamma4$, and $\gamma8$ would too be sensitive to the flop variant, while CNIH-2 would not. The structural basis for CKAMP44 modulation of AMPARs also awaits investigation, but our work points to an additive effect of splicing and CKAMPs on speeding entry into desensitization. Thus, our work establishes an intimate connection between TARPs/TARP-like proteins, entry into desensitization, and alternative splicing in the LBD.

Others have observed that AMPAR alternative splicing impacts TARP binding from both a structural and functional perspective. The stability of AMPAR-TARP complexes was assessed by co-IP, which indicated that TARP association was less stable with flop compared to flip receptors (Cais et al., 2014). The degree of TARP functional modulation on flip versus flop isoforms was noted to be different but has been largely overlooked with little mechanistic explanation (Turetsky et al., 2005; Bedoukian et al., 2006; Kott et al., 2007). Here, we provide kinetic insight into these distinctions and compare TARP $\gamma2$ to other prominent AMPAR auxiliary subunits.

Proteomics studies suggest that most native AMPARs are bound by at least two TARP molecules (Schwenk and Fakler, 2021), and thus it is tempting to envisage how allosteric coupling between the flip/flop cassette and TARPs may diversify native AMPAR signaling. Indeed, upon heteromerization, GluA1/A2 receptors exhibit a spectrum of responses shaped by flip/flop content and TARP stoichiometry that is consistent with AMPAR phenotypes from cerebellar Purkinje and stellate cells (Dawe et al., 2019). Interestingly, alternative splicing in the GluA2 subunit dictates the functional output of heteromer-TARP gating, consistent with GluA1 decay kinetics being relatively insensitive to splicing (Quirk et al., 2004). From a structural perspective, GluA2 occupies the position in AMPAR tetramers (i.e., B/D positions) that is the main TARP interacting site(s) in native complexes (Zhao et al., 2019). Thus, the privileged relationship between TARPs and alternative splicing, alluded to in this study, leads to the intriguing possibility of a dynamic interplay between TARP association and RNA processing that could, for example, be modified by changes in neuronal activity (Penn et al., 2012; Balik et al., 2013) as a means to fine-tune AMPAR-mediated excitatory transmission.

Alternative splicing of ion channel/auxiliary subunit complexes is widespread

The impact of alternative splicing is not unique to the AMPAR/auxiliary subunit complex but has also been observed in various voltage-gated channels. For example, the gene encoding the cardiac voltage-dependent L-type calcium channel (Cav1.2) is alternatively spliced at several loci, one of which generates variable N-termini. Alternative splicing in this region modifies regulation by both $\alpha_2\delta$ and β auxiliary subunits in terms of voltage sensitivity, current density, and/or decay kinetics (Cheng et al., 2007). A similar observation was recently made in the skeletal muscle voltage-gated calcium channel (Cav1.1). Regulation of Cav1.1 gating properties by the $\gamma1$ auxiliary subunit occurs in a splice variant-dependent manner. Specifically, $\gamma1$ reduced the current density in the adult Cav1.1a splice isoform but not in embryonic Cav1.1e, while $\gamma1$ modulation of steady-state inactivation and surface trafficking was unaffected by alternative splicing (El Ghaleb et al., 2022). Moreover, the α subunit of the neuronal sodium channel Nav1.7 is alternatively spliced at two sites, exon 5 and exon 11. Alternative splicing at exon 5 modulates the effect of $\beta1$ auxiliary subunits on the voltage-dependence of activation, while the length of exon 11 determines how $\beta1$ shifts the voltage-dependence of steady-state inactivation. Since splicing is evolutionarily conserved across sodium channel isoforms, it is possible that this type of regulation may be widespread (Farmer et al., 2012). Altogether, it is evident that alternative splicing and auxiliary subunit association confer an unprecedented complexity to the responsiveness of ion channels, allowing them to fulfill intricate, cell-specific signaling roles in the nervous system and beyond.

References

Balik A, Penn AC, Nemoda Z, Greger IH (2013) Activity-regulated RNA editing in select neuronal subfields in hippocampus. Nucleic Acids Res 41:1124–1134.

Bedoukian MA, Weeks AM, Partin KM (2006) Different domains of the AMPA receptor direct stargazin-mediated trafficking and stargazin-mediated modulation of kinetics. J Biol Chem 281:23908–23921.

Black DL (2000) Protein diversity from alternative splicing: a challenge for bioinformatics and post-genome biology. Cell 103:367–370.

Brown P, McGuire H, Bowie D (2018) Stargazin and cornichon-3 relieve polyamine block of AMPA receptors by enhancing blocker permeation. J Gen Physiol 150:67–82.

Cais O, Herguedas B, Krol K, Cull-Candy SG, Farrant M, Greger IH (2014) Mapping the interaction sites between AMPA receptors and TARPs reveals a role for the receptor N-terminal domain in channel gating. Cell Rep 9:728–740.

Chen S, Zhao Y, Wang Y, Shekhar M, Tajkhorshid E, Gouaux E (2017) Activation and desensitization mechanism of AMPA receptor-TARP complex by Cryo-EM. Cell 170:1234–1246.e14.

Cheng X, Liu J, Asuncion-Chin M, Blaskova E, Bannister JP, Dopico AM, Jaggar JH (2007) A novel Ca(V)1.2 N terminus expressed in smooth muscle cells of resistance size arteries modifies channel regulation by auxiliary subunits. J Biol Chem 282:29211–29221.

Coleman SK, Möykkynen T, Cai C, von Ossowski L, Kuismanen E, Korpi ER, Keinänen K (2006) Isoform-specific early trafficking of AMPA receptor flip and flop variants. J Neurosci 26:11220–11229.

Coombs ID, Soto D, Zonouzi M, Renzi M, Shelley C, Farrant M, Cull-Candy SG (2012) Cornichons modify channel properties of recombinant and glial AMPA receptors. J Neurosci 32:9796–9804.

Dawe GB, Musgaard M, Aurousseau MRP, Nayeem N, Green T, Biggin PC, Bowie D (2016) Distinct structural pathways coordinate the activation of AMPA receptor-auxiliary subunit complexes. Neuron 89:1264–1276.

Dawe GB, Kadir MF, Venskutonyte R, Perozzo AM, Yan Y, Alexander RPD, Navarrete C, Santander EA, Arsenault M, Fuentes C, Aurousseau MRP, Frydenvang K, Barrera NP, Kastrup JS, Edwardson JM, Bowie D (2019) Nanoscale mobility of the Apo state and TARP stoichiometry dictate the gating behavior of alternatively spliced AMPA receptors. Neuron 102:976–992.e5.

Dredge BK, Polydorides AD, Darnell RB (2001) The splice of life: alternative splicing and neurological disease. Nat Rev Neurosci 2:43–50.

El Ghaleb Y, Ortner NJ, Posch W, Fernandez-Quintero ML, Tuinte WE, Monteleone S, Draheim HJ, Liedl KR, Wilflingseder D, Striessnig J, Tuluc P, Flucher BE, Campiglio M (2022) Calcium current modulation by the gamma1 subunit depends on alternative splicing of CaV1.1. J Gen Physiol 154:e202113028.

Farmer C, Cox JJ, Fletcher EV, Woods CG, Wood JN, Schorge S (2012) Splice variants of Na(V)1.7 sodium channels have distinct β subunit-dependent biophysical properties. PLoS One 7:e41750.

Grabowski PJ, Black DL (2001) Alternative RNA splicing in the nervous system. Prog Neurobiol 65:289–308.

Hansen KB, Wollmuth LP, Bowie D, Furukawa H, Menniti FS, Sobolevsky AI, Swanson GT, Swanger SA, Greger IH, Nakagawa T, McBain CJ, Jayaraman V, Low CM, Dell'Acqua ML, Diamond JS, Camp CR, Perszyk RE, Yuan H, Traynelis SF (2021) Structure, function, and pharmacology of glutamate receptor ion channels. Pharmacol Rev 73:1469– 1658.

Hawken NM, Zaika EI, Nakagawa T (2017) Engineering defined membrane-embedded elements of AMPA receptor induces opposing gating modulation by cornichon 3 and stargazin. J Physiol 595:6517–6539.

Herbrechter R, Hube N, Buchholz R, Reiner A (2021) Splicing and editing of ionotropic glutamate receptors: a comprehensive analysis based on human RNA-Seq data. Cell Mol Life Sci 78:5605–5630.

Hood JL, Emeson RB (2012) Editing of neurotransmitter receptor and ion channel RNAs in the nervous system. Curr Top Microbiol Immunol 353:61–90.

Howe JR (2015) Modulation of non-NMDA receptor gating by auxiliary subunits. J Physiol 593:61–72.

Jackson AC, Nicoll RA (2011) The expanding social network of ionotropic glutamate receptors: TARPs and other transmembrane auxiliary subunits. Neuron 70:178–199.

Jones MV, Westbrook GL (1996) The impact of receptor desensitization on fast synaptic transmission. Trends Neurosci 19:96–101.

Kamalova A, Nakagawa T (2021) AMPA receptor structure and auxiliary subunits. J Physiol 599:453–469.

Koike M, Tsukada S, Tsuzuki K, Kijima H, Ozawa S (2000) Regulation of kinetic properties of GluR2 AMPA receptor channels by alternative splicing. J Neurosci 20:2166–2174.

Kott S, Werner M, Körber C, Hollmann M (2007) Electrophysiological properties of AMPA receptors are differentially modulated depending on the associated member of the TARP family. J Neurosci 27:3780–3789.

Li Q, Lee JA, Black DL (2007) Neuronal regulation of alternative pre-mRNA splicing. Nat Rev Neurosci 8:819–831.

Lipscombe D (2005) Neuronal proteins custom designed by alternative splicing. Curr Opin Neurobiol 15:358–363.

Lipscombe D, Andrade A, Allen SE (2013) Alternative splicing: functional diversity among voltage-gated calcium channels and behavioral consequences. Biochim Biophys Acta 1828:1522–1529.

Matthews PM, Pinggera A, Kampjut D, Greger IH (2021) Biology of AMPA receptor interacting proteins - from biogenesis to synaptic plasticity. Neuropharmacology 197:108709.

McGee TP, Bats C, Farrant M, Cull-Candy SG (2015) Auxiliary subunit GSG1L acts to suppress calcium-permeable AMPA receptor function. J Neurosci 35:16171–16179.

Meyerson JR, Kumar J, Chittori S, Rao P, Pierson J, Bartesaghi A, Mayer ML, Subramaniam S (2014) Structural mechanism of glutamate receptor activation and desensitization. Nature 514:328–334.

Monyer H, Seeburg PH, Wisden W (1991) Glutamate-operated channels: developmentally early and mature forms arise by alternative splicing. Neuron 6:799–810.

Mosbacher J, Schoepfer R, Monyer H, Burnashev N, Seeburg PH, Ruppersberg JP (1994) A molecular determinant for submillisecond desensitization in glutamate receptors. Science 266:1059–1062.

Nakagawa T (2019) Structures of the AMPA receptor in complex with its auxiliary subunit cornichon. Science 366:1259–1263.

Orlandi C, La Via L, Bonini D, Mora C, Russo I, Barbon A, Barlati S (2011) AMPA receptor regulation at the mRNA and protein level in rat primary cortical cultures. PLoS One 6:e25350.

Partin KM, Patneau DK, Mayer ML (1994) Cyclothiazide differentially modulates desensitization of alpha-amino-3-hydroxy-5-methyl-4-isoxazolepropionic acid receptor splice variants. Mol Pharmacol 46:129–138.

Partin KM, Fleck MW, Mayer ML (1996) AMPA receptor flip/flop mutants affecting deactivation, desensitization, and modulation by cyclothiazide, aniracetam, and thiocyanate. J Neurosci 16:6634–6647.

Penn AC, Williams SR, Greger IH (2008) Gating motions underlie AMPA receptor secretion from the endoplasmic reticulum. EMBO J 27:3056–3068.

Penn AC, Balik A, Wozny C, Cais O, Greger IH (2012) Activity-mediated AMPA receptor remodeling, driven by alternative splicing in the ligand-binding domain. Neuron 76:503–510.

Priel A, Kolleker A, Ayalon G, Gillor M, Osten P, Stern-Bach Y (2005) Stargazin reduces desensitization and slows deactivation of the AMPA-type glutamate receptors. J Neurosci 25:2682–2686.

Quirk JC, Siuda ER, Nisenbaum ES (2004) Molecular determinants responsible for differences in desensitization kinetics of AMPA receptor splice variants. J Neurosci 24:11416–11420.

Raman IM, Trussell LO (1995) The mechanism of alpha-amino-3-hydroxy-5-methyl-4-isoxazolepropionate receptor desensitization after removal of glutamate. Biophys J 68:137–146.

Riva I, Eibl C, Volkmer R, Carbone AL, Plested AJ (2017) Control of AMPA receptor activity by the extracellular loops of auxiliary proteins. Elife 6: e28680.

Schmid S, Guthmann A, Ruppersberg JP, Herbert H (2001) Expression of AMPA receptor subunit flip/flop splice variants in the rat auditory brainstem and inferior colliculus. J Comp Neurol 430:160–171.

Schwenk J, Fakler B (2021) Building of AMPA-type glutamate receptors in the endoplasmic reticulum and its implication for excitatory neurotransmission. J Physiol 599:2639–2653.

Schwenk J, Harmel N, Brechet A, Zolles G, Berkefeld H, Müller CS, Bildl W, Baehrens D, Hüber B, Kulik A, Klöcker N, Schulte U, Fakler B (2012) High-resolution proteomics unravel architecture and molecular diversity of native AMPA receptor complexes. Neuron 74:621–633.

Seeburg PH (1996) The role of RNA editing in controlling glutamate receptor channel properties. J Neurochem 66:1–5.

Shanks NF, Savas JN, Maruo T, Cais O, Hirao A, Oe S, Ghosh A, Noda Y, Greger IH, Yates JR, 3rd, Nakagawa T (2012) Differences in AMPA and

kainate receptor interactomes facilitate identification of AMPA receptor auxiliary subunit GSG1L. Cell Rep 1:590–598.

Shi Y, Suh YH, Milstein AD, Isozaki K, Schmid SM, Roche KW, Nicoll RA (2010) Functional comparison of the effects of TARPs and cornichons on AMPA receptor trafficking and gating. Proc Natl Acad Sci U S A 107:16315–16319.

Sommer B, Keinänen K, Verdoorn TA, Wisden W, Burnashev N, Herb A, Köhler M, Takagi T, Sakmann B, Seeburg PH (1990) Flip and flop: a cell-specific functional switch in glutamate-operated channels of the CNS. Science 249:1580–1585.

Sukumaran M, Penn AC, Greger IH (2012) AMPA receptor assembly: atomic determinants and built-in modulators. Adv Exp Med Biol 970:241–264.

Sun Y, Olson R, Horning M, Armstrong N, Mayer M, Gouaux E (2002) Mechanism of glutamate receptor desensitization. Nature 417:245–253.

Swanson GT, Kamboj SK, Cull-Candy SG (1997) Single-channel properties of recombinant AMPA receptors depend on RNA editing, splice variation, and subunit composition. J Neurosci 17:58–69.

Trussell LO (1997) Cellular mechanisms for preservation of timing in central auditory pathways. Curr Opin Neurobiol 7:487–492.

Trussell L (1998) Control of time course of glutamatergic synaptic currents. Prog Brain Res 116:59–69.

Turetsky D, Garringer E, Patneau DK (2005) Stargazin modulates native AMPA receptor functional properties by two distinct mechanisms. J Neurosci 25:7438–7448.

Twomey EC, Yelshanskaya MV, Grassucci RA, Frank J, Sobolevsky AI (2016) Elucidation of AMPA receptor-stargazin complexes by cryo-electron microscopy. Science 353:83–86.

Twomey EC, Yelshanskaya MV, Grassucci RA, Frank J, Sobolevsky AI (2017) Structural Bases of Desensitization in AMPA Receptor-Auxiliary Subunit Complexes. Neuron 94:569–580.e5.

Twomey EC, Yelshanskaya MV, Sobolevsky AI (2019) Structural and functional insights into transmembrane AMPA receptor regulatory protein complexes. J Gen Physiol 151:1347–1356.

von Engelhardt J, Mack V, Sprengel R, Kavenstock N, Li KW, Stern-Bach Y, Smit AB, Seeburg PH, Monyer H (2010) CKAMP44: a brain-specific protein attenuating short-term synaptic plasticity in the dentate gyrus. Science 327:1518–1522.

Vuong CK, Black DL, Zheng S (2016) The neurogenetics of alternative splicing. Nat Rev Neurosci 17:265–281.

Yu J, Rao P, Clark S, Mitra J, Ha T, Gouaux E (2021) Hippocampal AMPA receptor assemblies and mechanism of allosteric inhibition. Nature 594:448–453.

Zhang D, Watson JF, Matthews PM, Cais O, Greger IH (2021) Gating and modulation of a hetero-octameric AMPA glutamate receptor. Nature 594:454–458.

Zhang W, Devi SP, Tomita S, Howe JR (2014) Auxiliary proteins promote modal gating of AMPA- and kainate-type glutamate receptors. Eur J Neurosci 39:1138–1147.

Zhao Y, Chen S, Swensen AC, Qian WJ, Gouaux E (2019) Architecture and subunit arrangement of native AMPA receptors elucidated by cryo-EM. Science 364:355–362.